Video Article

Experimental Multiscale Methodology for Predicting Material Fouling Resistance

Pavlina Karafillis[1], Abdulla Alhajri[2], Vikash Mishra[3], Leigh Lin[1], Rasheed Auguste[2], Gabrielle Ledoux[2], Alan Schwartzman[4], Ekaterina Paramonova[2], Michael Philip Short[2]

[1]Department of Mechanical Engineering, Massachusetts Institute of Technology

[2]Department of Nuclear Science and Engineering, Massachusetts Institute of Technology

[3]Department of Mechanical Engineering, University of Arkansas

[4]Department of Materials Science and Engineering, Massachusetts Institute of Technology

Correspondence to: Michael Philip Short at hereiam@mit.edu

URL: http://www.jove.com/video/52952
DOI: doi:10.3791/52952

Keywords: Fouling, adhesion, CRUD, nuclear, nuclear materials, pool boiling, AFM, AFM-FS, force spectroscopy

Date Published: 3/10/2016

Citation: Karafillis, P., Alhajri, A., Mishra, V., Lin, L., Auguste, R., Ledoux, G., Schwartzman, A., Paramonova, E., Short, M.P. Experimental Multiscale Methodology for Predicting Material Fouling Resistance. *J. Vis. Exp.* (), e52952, doi:10.3791/52952 (2016).

Abstract

The buildup of fouling deposits in energy systems degrades their ability to transfer heat, reducing efficiency and causing operational issues such as localized corrosion. Each application presents its own challenges. In nuclear power generation, the buildup of CRUD (Chalk River Unidentified Deposits) induces unique, negative effects ranging from reduced heat transfer, to axial power shifting, to CRUD-induced localized corrosion (CILC), the last of which can cause sudden fuel failure. Knowledge of why CRUD forms and how to prevent its adhesion to nuclear fuel rods represents a major step towards eliminating it. This paper demonstrates a methodology to ascertain which materials may resist CRUD adhesion, thereby preventing its initiation and growth. It presents experiments targeted at multiple length scales: pool boiling (macroscale), which simulates CRUD initiation processes in a nuclear reactor, and atomic force microscope (AFM) force spectroscopy (microscale), which yields quantitative measurements of the adhesion between CRUD constituents and candidate CRUD-resistant materials. Early data from both sets of experiments show some correlation, suggesting that AFM force spectroscopy (AFM-FS) may be used to pre-screen materials for fouling resistance. So far, it appears that CRUD constituents adhere well to oxides, while carbides show both greatly reduced adhesion and no adherent CRUD in pool boiling experiments. The relationship between the AFM-FS measurements and the growth of CRUD in the pool boiling experiments may provide insight into the possible factors affecting fouling in nuclear reactors, eventually leading to its elimination.

Introduction

Fouling, or the unwanted buildup of corrosion products on a surface, complements corrosion as a surface-based material degradation mechanism. Fouling is particularly detrimental in energy systems, as the surfaces which transfer the most enthalpy are typically the most susceptible. In essence, the presence of fouling deposits, often porous and/or thermally insulating, impedes the efficient flow of heat through a system. The high flow rates and large temperature differences in the hot and cold sections of a heat transfer system or coolant loop provide ideal environments to induce flow-assisted corrosion, and subsequent transport of corrosion products from areas producing soluble & particulate species, to the areas in which deposition is most favorable. In most energy systems, corrosion is most severe in the hottest sections of a coolant loop, since corrosion rates often accelerate exponentially with temperature. In the case of systems undergoing boiling, however, the formation and cavitation of bubbles on a material surface may induce species precipitation via microlayer dryout underneath bubbles. Here the growth of fouling deposits can be particularly rapid, and the resultant effects unusually devastating. Economically, heat exchanger fouling costs many industrial countries roughly 0.25% of its gross domestic product in annual lost productivity due to fluid treatment, cleaning, component replacement, and loss of production [1], equivalent to approximately $42 billion in the United States. Figures for worldwide industries such as boilers, marine shipping, and oil/gas production are far higher.

In nuclear light water reactors (LWRs), foulants composed of soluble and particulate nickel- and iron-bearing species deposit on fuel cladding rods to form CRUD, or Chalk River Unidentified Deposits. CRUD takes the form of highly porous deposits roughly tens to one hundred microns thick, with porosities on the order of 50%. In pressurized water reactors (PWRs), CRUD is largely formed from deposits of nickel ferrites ($Ni_xFe_{3-x}O_4$) in addition to small amounts of NiO, Ni metal, and some iron and nickel chromites ($FeCr_2O_4$, $NiCr_2O_4$, and $Ni_xFe_{1-x}Cr_2O_4$) [1,19]. Images of CRUD at different length scales are shown in **Figure 1**. [2] It takes the form of brownish-grey deposits on fuel rods, which when viewed in cross section exhibits multiple, self-similar length scales of porosity. The larger pores, known as "boiling chimneys," provide a path for vaporized water to escape the CRUD, while the smaller pores throughout serve to draw water within. This porous network of CRUD normally draws water into its pores via capillary action, but dryout may occur for very high values of heat flux. The smallest constituents of CRUD are particles, some crystalline, of the iron-nickel-chromium oxides which form the nanoporous framework. Zinc oxides and zirconium oxide are also sometimes present in CRUD.

CRUD can cause multiple negative side effects in PWRs, including CRUD-induced localized corrosion (CILC), which can lead to sudden fuel failure, elevated cladding temperatures due to CRUD's additional thermal resistance, and downward axial power shifts in the reactor [9]. Previous studies [3] have shown that Zircaloys (of which PWR fuel cladding is made) corrode far more quickly at elevated temperatures. Recent

multiphysics modeling efforts [4] have shown that the presence of CRUD tens of microns thick can elevate cladding temperatures by 15°C, which corresponds to roughly a doubling of the corrosion rate. The last problem of axial power shifting is due to the accumulation of boron, present to control the neutron population in the reactor, in the pores of the CRUD. Recent massively parallel, multiphysics simulations of CRUD's effects [5] demonstrated this effect by simulating CRUD formation and boron accumulation along 3,000 fuel rods in a reactor, demonstrating a downward shit in reactor power. This behavior was already known from nuclear plant measurements [6].

Previous attempts have been made to develop materials resistant to CRUD formation. Solutions have included manipulating the growth of CRUD to improve heat transfer [10], manipulating water chemistry to minimize CRUD growth and corrosion [11], pretreating zircaloy [12], and using magnetic separation as a filtration system [21]. One recent patent [7] proposed to electropolish fuel cladding surfaces, to remove nucleation sites for bubbles which can induce CRUD. However, so far no method has resulted in completely preventing the growth of CRUD. We believe that uncovering the mechanism of the initiation event of CRUD formation, the adhesion of the first particles to a substrate, is the key to preventing its formation altogether. Therefore, precise measurement of surface adhesion forces, along with proof-of-principle experiments at higher length scales, is required to predict and confirm the fouling resistance of candidate materials.

This paper presents an experimental, multiscale methodology to discover materials that can be applied to nuclear fuel cladding and prevent the growth of CRUD. In order to achieve this goal, a variety of materials are being tested, shown in **Table 1,** representing different classes of potential anti-fouling and model materials. First, sputtered or grown specimens of each material are exposed an environment similar to that of a nuclear reactor, specifically a PWR (Pressurized Water Reactor), and "cooked," or indirectly heated to induce pool boiling with excess amount of CRUD forming particulates (NiO and Fe_3O_4) to simulate the boiling process on the surfaces of nuclear fuel rods. The cooked samples containing simulated CRUD are then imaged top-down using a high-resolution scanning electron microscope (SEM) and in cross section using a focused ion beam (FIB), allowing for visualization of any CRUD-substrate bond that may be present.

The experimental pool boiling setup that has been developed possesses certain unique benefits that make experiments repeatable, effective, and more representative of in-reactor conditions. A vertically oriented sample holder, as shown in **Figure 2** prevents nickel- and iron-based particulates that fall out of solution from depositing on the surface of the sample by gravity. Strongly sonicating the CRUD-bearing solution prior to the experiment allows for longer test times and less precipitation of particulates. In addition, for each of the four samples being tested, the heat flux and temperature is recorded throughout the experiment. The pH of the simulated PWR water is also recorded throughout the experiment.

In order to quantify the bond between the CRUD deposits and the surface, we also perform AFM force spectroscopy (AFM-FS) measurements in both air and simulated PWR water on clean surfaces of the same materials. First, AFM cantilevers are functionalized with particles made of one micron spheres of compounds commonly found in CRUD (NiO or Fe_3O_4). In the MFP3D-BIO, the AFM used in this procedure, the cantilever is modeled so that the force applied to the cantilever tip is proportional to its deflection when in contact with the surface. A laser reflects off the cantilever to a photodetector to measure its deflection. In the procedure below, two constants, the spring constant and the deflection InvOLS (inverse optical lever sensitivity) must be calibrated in order to convert the deflection read by the photodetector to nanoNewtons.

In order to record adhesion of the tip to the surface, the cantilever tip is pressed against the surface of the sample with a force of 25nN. In the experiments recorded below, the tip will then remain at the surface for a period of either 0, 5, 10, 30, or 60 seconds. As the cantilever is being retracted, the tip will often adhere to the sample surface, causing the cantilever to deflect until the force of the cantilever deflection is greater than the adhesion between the CRUD particle and the surface under investigation. Then the cantilever snaps back to zero deflection. It is this maximum deflection, and its corresponding adhesion force, that the AFM can quickly and repetitively record [18]. The area under the force-distance curve produced by AFM-FS is a direct measure of the work of separation between CRUD and a substrate, and therefore quantitatively estimates the adhesion of that CRUD particle to each surface. Using the same AFM cantilever on multiple samples eliminates variability in particulate size and composition.

This unique combination of simulated CRUD growth and AFM measurements provides multiple, coupled datasets that allow us to understand how and why CRUD may develop on certain material surfaces. Rather than undergo time-consuming pool boiling experiments, which can take up to a day to complete, a large number of materials can be pre-screened using AFM-FS to estimate their fouling resistance. We also show initial results confirming the efficacy of this procedure, whereby materials which exhibit little to no CRUD adhesion in pool boiling also show very low values of CRUD-substrate adhesion in AFM-FS. Conversely, materials which grow large amounts of adherent CRUD in pool boiling also adhere strongly to CRUD particles in the AFM.

Protocol

1. Material Preparation

1. Using a suitable machining method, section 1 cm x 1 cm coupons of the base substrate material (here, Zircaloy-4) from a sheet approximately 1 mm thick. The exact thickness is not important.
2. Using a manual or automatic polishing machine, polish the base substrates to an optically smooth, mirror finish.
    1. Mount specimens to a flat sample holder using a hot plate and a shear-resistant wax, for insertion into an automatic grinding/polishing machine. Here, mount twenty at once.
    2. Grind the faces of the mounted samples smooth on a rough diamond grinding disc (DGD) or with coarse sandpaper mounted to a very flat platen.
    3. Remove the samples from the sample holder by carefully chiseling the side of each sample with a flathead screwdriver. The mounting adhesive should cleave and break off with very little force.
    4. Sonicate the samples in acetone for 5 minutes, then in 100% ethanol for 5 minutes to remove any trace of the mounting adhesive.
    5. Mount the newly flattened faces of the same samples to the flat sample holder using the mounting adhesive.
    6. Using successively finer grit sandpaper or diamond solutions, polish the faces of each sample.
        1. First, flatten the exposed faces of the samples using the DGD or coarse sandpaper.

2. Next, use ~240 grit sandpaper to remove all the scratches from the previous polishing step. Polish for at least one minute using water as a lubricant, or until all scratches from the rough grinding stage are removed.
3. Remove the sample holder with samples from the polishing machine. Sonicate the entire assembly for at least two minutes, to remove any embedded sandpaper grit. If the entire assembly does not fit in the sonicator, rotate the assembly in the water, sonicating each section for at least two minutes. Return the assembly to the polishing machine.
4. Repeat steps 1.2.6.2-1.2.6.3 with 400 grit and 800 grit sandpaper.
5. If not wearing gloves, put them on at this stage. Diamond particles and silica nanoparticles can lodge under the skin, and are very uncomfortable!
6. Use a 9 µm diamond suspension on a suitable polishing cloth, without additional water lubricant, to continue polishing the specimen. Squirt or pour a small amount (5-10 mL) of diamond suspension on the spinning platen once every 15-30 seconds. Repeat step 1.2.6.3.
7. Repeat steps 1.2.6.6-1.2.6.7 for 3 µm and 1 µm diamond suspensions.
8. Using a 0.05 µm silica suspension and a clean, appropriately chosen polishing cloth, polish the samples to an absolute mirror finish. This may take up to 30 minutes.
9. Clean any excess silica suspension from the samples using squirt bottles of ethanol and lint-free wipes or lens cloth.

7. Repeat steps 1.2.4-1.2.5.

3. Using a suitable surface deposition method for each of the materials, deposit the chosen potentially CRUD-resistant materials onto the mirror-finished sides of the base substrates. Here, use sputtering for the materials. Sputter the materials to test to a thickness of approximately 50 nm. The exact thickness is not important, as long as it is sufficiently thick to discount any changes in surface chemistry from its underlying substrate.

2. Cooking sample

1. PWR Water Preparation
   1. First, prepare simulated PWR reactor water. Measure 5 L of deionized water, 0.06 g of boric acid and 0.03 g of lithium hydroxide. Mix together and shake vigorously. This 'simulated PWR water' can be used in later experiments.

2. Measure 0.18 g of NiO nanoparticles (10-50 nm), 0.18 g of Fe_3O_4 nanoparticles (10-50 nm), and 300 mL of deionized water. Mix together these CRUD particulates in a beaker.
3. Add 200 mL of simulated PWR reactor water to the solution with CRUD particulates. Strongly sonicate the solution for 5 minutes.
   Note: The simulated PWR water consists of 10 ppm of H_3BO_3, 5 ppm of LiOH, 100 ppm of NiO and 100 ppm of Fe_3O_4 and 1.8 L of deionized (>15 MΩ) water. These measurements may change depending on desired ratios of particulates and experimental chamber size. Normal concentrations of NiO and Fe_3O_4 in PWRs are 10's to 100's of ppb. [4]

3. Cooking Preparation

1. If the simulated PWR water is not freshly mixed, turn the container of simulated PWR water on its head. This helps eliminate the acidity gradient that tends to develop when the simulated PWR water sits for long periods of time.
2. Cover both sides of each heat flux sensor with a thin layer of conductive silver paste. This helps ensure good thermal conduction into the sample. Use as little as possible, to prevent the entry of silver paste into the simulated PWR water in the pool boiling facility. Remember to check for silver's presence in the CRUD using a suitable technique (SEM/EDX) later.
3. Place a clean, sample on top of each heat flux sensor. If not all heat flux sensors will be used, cover these unused ones with a thin piece of rubber.
4. Place and clamp down an insulating material on all exposed metal surfaces in contact with the heating element to prevent boiling on surfaces other than sample itself.
5. Place O-ring on experimental body. Put some silicon grease in the O-ring groove to keep the O-ring in place while the nuts are beings tightened. Tighten the nuts.
6. Insert pH probe and water bath thermocouple.
7. Pour in the sonicated nanoparticle solution and an additional 1.3 L of the simulated PWR water. Make sure that there is a vent for the displaced air to exit. Once the sample holder and pump intake has been completely covered by PWR water, seal off the experimental body.

4. Cooking

1. Turn on the data collection system and the circulation pump to a flow rate of approximately 130 mL/min.
   Note: The pump promotes sub-nucleate boiling by preventing the formation of a vapor film with a steady stream of water. The data collection system records heat flux for each sample, bath temperature, each sample temperature, and the system pH. A credit card sized data logging circuit board and its carrier board with screw-type terminal block connections is used as a data collection device, and K-type thermocouple measurements are amplified by a simple circuit presented in **Figure 3**.
2. Turn on the Proportional Integral Derivative (PID) bath heater controller, with a set point of 97 °C.
   Note: The circuit diagram of the control box that houses the pH meter, and the PID bath and sample controllers is presented in **Figure 4**. The bath water should not reach over 97 °C. The bath water temperature and the sample temperature difference should not be greater than 10 °C while the sample heater is off. A large temperature discrepancy during heating can cause excessive CRUD growth and affect the repeatability of the results.
3. After the water has reached a temperature of 90 °C, turn on the PID sample heater controller. The sample should quickly stabilize at 125 °C.
4. Create new file in the data collection system to record experimental conditions of sample & bath temperatures, pH, and heat flux. Begin data collection as soon as the samples stabilize at 125 °C.

5. Let the experiment run for the desired amount of time. Typically, runs last from 15 minutes to 8 hours.

5. Clean-up

1. At the end of desired run time, turn off all heaters.
2. Drain the experimental body, collecting a sample of water for records and possible future chemical analyses. Label properly.
3. Place paper towels underneath the experimental body, untighten, and remove nuts.
4. Unscrew the rubber cover at the center of the sample holder. Unclamp and remove Teflon cap.
5. Carefully retrieve and store cooked samples. These samples are ready to be examined using the SEM, or any other analysis technique.

6. Atomic Force Microscopy Force Spectroscopy in PWR Water

1. **Calibrate the Spring Constant Photodiode Resonse of the Cantilever**
    1. Load a CRUD-functionalized tip into the cantilever holder.
        1. To do so, loosen the screws on the spring clip. Using two tweezers, hold the cantilever and raise the spring clip. Slide a CRUD-functionalized AFM cantilever under the spring clip and tighten the screws on the spring clip. Make sure that the cantilever tip is one half to two thirds up the trapezoidal window on the cantilever holder and parallel to the top of the trapezoidal window.
        2. Load the cantilever holder into the AFM head.
    2. Turn on the top-down optics system to view the top of the AFM cantilever.
    3. Clean a glass slide with MeOH (methanol). Place it onto the stage and return the AFM head back on the stage.
    4. Align the laser on the cantilever tip and maximize the reported sum.
    5. Adjust the photodetector until the deflection reads zero volts.
    6. Select 'engage' to electronically lower the cantilever. Slowly lower the front of the AFM head manually until the cantilever tip engages with the surface of the glass slide. Continue to lower the front of the AFM head until the voltage of the z-piezo is 70 V at the surface of the slide.
    7. Withdraw the cantilever and adjust the photodetector until the deflection is 0 V +/-0.09 when the tip is withdrawn. Repeat steps 6.1.6 and 6.1.7 until the correct voltages are achieved.
    8. Calibrate the photodiode response or (volts) per nanometer of cantilever deflection. Complete a single force curve and a linear fit to find the inverse slope of the force curve while the cantilever is in contact with the glass slide. The reciprocal of the slope is the photodiode response.
    9. Disengage the tip from the surface.
    10. Begin capturing thermal data. During this process, the thermal vibration of the cantilever is recorded. The AFM software analyzes a power spectrum of the thermal vibration and plots it in a new window.
    11. Wait for the sample collection count to reach over 100, then stop the data collection. Use the AFM software to specify the center and width of the lowest-frequency (fundamental resonance) peak.
    12. Perform a fit to determine the spring constant.[23]
    13. If AFM-FS measurements in air are desired, skip to step 6.3. Otherwise proceed with step 6.2 first to perform AFM-FS measurements in water.

2. **Calibrating AFM in Water**
    1. Raise the AFM head, take it off the stage, and place it cantilever-side up. Use a pipette incremented to at least 20 µL to place one or two drops of the simulated PWR water on the cantilever tip, but no more than 20 µL.
    2. Place no more than 60 µL of the simulated PWR water on the glass slide. Return the AFM head to the stage. Make sure the water on the sample and the water on the cantilever form one droplet.
    3. Realign the laser beam on the back of the cantilever tip and maximize the reported sum. Due to Snell's law, the laser will refract in the water and will therefore have to be realigned.
    4. Repeat steps 6.1.5 through 6.1.8 to engage the tip with the surface and calibrate the photodiode response.
    Note: The simulated PWR water in this procedure has a pH greater than 5.5 and less than 8. If the water pH exceeds this range, a different cantilever holder must be used.

3. **Collecting Force Maps**
    1. Raise the AFM head by more than the height of the sample to make sure the cantilever won't crash with the sample surface when the AFM head is reinstalled. Remove the AFM head and glass slide from the stage.
    2. Clean a glass slide with MeOH and secure the sample to the surface with double sided tape. Place the sample on the stage. For AFM measurements in water, place no more than 60 µL of simulated PWR water on the surface of the sample and one or two drops of simulated PWR water on the cantilever. Reinstall the AFM head making sure that the water droplets on the tip and on the sample surface meet and coalesce.
    3. Engage the AFM tip with the sample surface as described in 6.1.6.
    4. If ringing occurs, where the deflection oscillates quickly over large ranges, particularly from positive to negative, decrease the integral gain.
    5. Set the force distance and start distance by engaging the tip with the surface, and right-clicking the red bar on the force calibration screen. Select the dwell type 'towards surface' and a desired dwell time. Set the velocity to approximately 2 µm/sec and the trigger point (the force applied by the tip to the surface) to 25 nN.
    6. Define a 6 x 6 grid (or greater grid for better statistics) with a scan size to be 15 µm.
    7. Click 'Do Scan' to collect the number of force curves specified in the grid.
    8. Repeat steps 6.3.6-6.3.7 at different locations at least 30 µm apart with varying dwell times.

7. Clean Up

1. Remove the AFM head, the sample, and the glass slide from the stage. Store the sample and clean the glass slide.
2. Remove the cantilever holder and carefully wick up the remaining solution off the cantilever, if desired. Remove the cantilever and place it in a gel pack or reusable storage container.
3. Clean the cantilever holder with MeOH.

Representative Results

Initial results show that experiments in both the pool boiling facility and the AFM-FS measurements show some correspondence. Materials which grew visually adherent CRUD in pool boiling exhibited high values of adhesion in AFM-FS, while materials on which CRUD did not grow exhibit low values of adhesion in AFM-FS. In addition, the average adhesion force vs. dwell time increased for materials on which CRUD grew, while potential CRUD-resistant materials did not exhibit this increase.

Section 1.1: SEM/FIB Images

Figure 5 shows an SEM image from the FIB of CRUD grown on a sample of TiO_2, cooked in the experimental facility shown similar to **Figure 2,** except the sample was oriented horizontally, and there was only one sample in the chamber rather than four. This image clearly shows adherence between the simulated CRUD and the TiO_2 substrate. **Figure 6** shows an image of a sample of CRUD-like particles deposited on ZrC. This image shows the limited bonding between the ZrC and the CRUD. In particular, one should notice that the CRUD on TiO_2 is strongly adherent to the substrate, leaving no porosity between CRUD and TiO_2. By contrast, the CRUD particles on ZrC are clearly not adhered to the substrate, rather they simply sit on the exposed surface. No adhered CRUD particles were present on this sample. The horizontal orientation of the sample surfaces presented in this paper explains the presence of large pieces of CRUD that are sitting on but not adhered to the surface of the sample. These particles likely deposited from the simulated PWR water with nanoparticles clustering and settling out of solution, without adhesion. During the experiment, CRUD particles can come out of PWR solution and drift down to the sample surface when the sample is horizontally oriented. The vertical orientation should eliminate this problem. **Figure 7** shows evidence that the larger sediments on the sample surface are not adhered to the surface, as an omniprobe in the FIB easily moved them with a little prodding.

Section 1.2: AFM-FS Measurements

Figure 8 shows a single sample force curve [13]. The x-axis reflects the tip distance from the surface of the sample, and the y-axis records the force felt by the tip, which is proportional to the deflection of the cantilever. A positive force corresponds to the tip being pushed by the sample surface and a negative force to the tip being pulled by the sample surface, but still held on by adhesion forces. The black line records the approach, while the red line records the retraction of the sample from the surface. This graph also presents effects of electrostatic forces as the sample approaches. Particularly for the AFM tips with NiO in air, electrostatic forces had a significant effect on the force during the approach, causing significant deflection away from (negative force) or towards the sample surface (positive force) until it contacted the surface. Therefore, data using Fe_3O_4 functionalized AFM cantilevers will be presented in this section, as these electrostatic effects were not observed as strongly. The adhesion data recorded is the difference between zero deflection, and the minimum force felt by the cantilever.

Figures 9 and **11** present the AFM-FS in-air data based on dwell time at the surface for TiO_2 and ZrC surfaces with Fe_3O_4 tips. For TiO_2, average adhesion increases with increasing dwell time, while the ZrC presents the opposite result. In addition, the measured adhesion forces, in both air and water, are visibly greater for TiO_2. **Figures 10** and **12** present similar data, but performed in a droplet of simulated PWR water. Here, the average adhesion of the ZrC is also consistently less than in adhesion of the TiO_2. It is important to note the change of scale on the y-axis and the significant decrease in adhesion force between air and water. All AFM data points, except those with a dwell time of 60 seconds are the average of 36 adhesion measurements. Data points with dwell times of 60 seconds are the average of 16 adhesion measurements.

LWR Materials	Model Materials	New Materials	Geometric Mods
	Au	Tetragonal ZrO_2	
	Ag	Monoclinic ZrO_2	Nucleation sites
Native Zircaloy-4	SiO_2	ZrN	Micropillars
100nm ZrO_2	Al_2O_3	ZrC	Hydrophobic coatings
2μm ZrO_2	MgO	ZrB_2	Hydrophilic coatings
	Diamond-like carbon (DLC)	Ti-equivalents (TiN, TiC, TiB_2)	Biphilic coatings
	Graphene	CeO_2	

Table 1: Materials and surface modifications considered in this study. Materials referred to in this study are shown in bold.

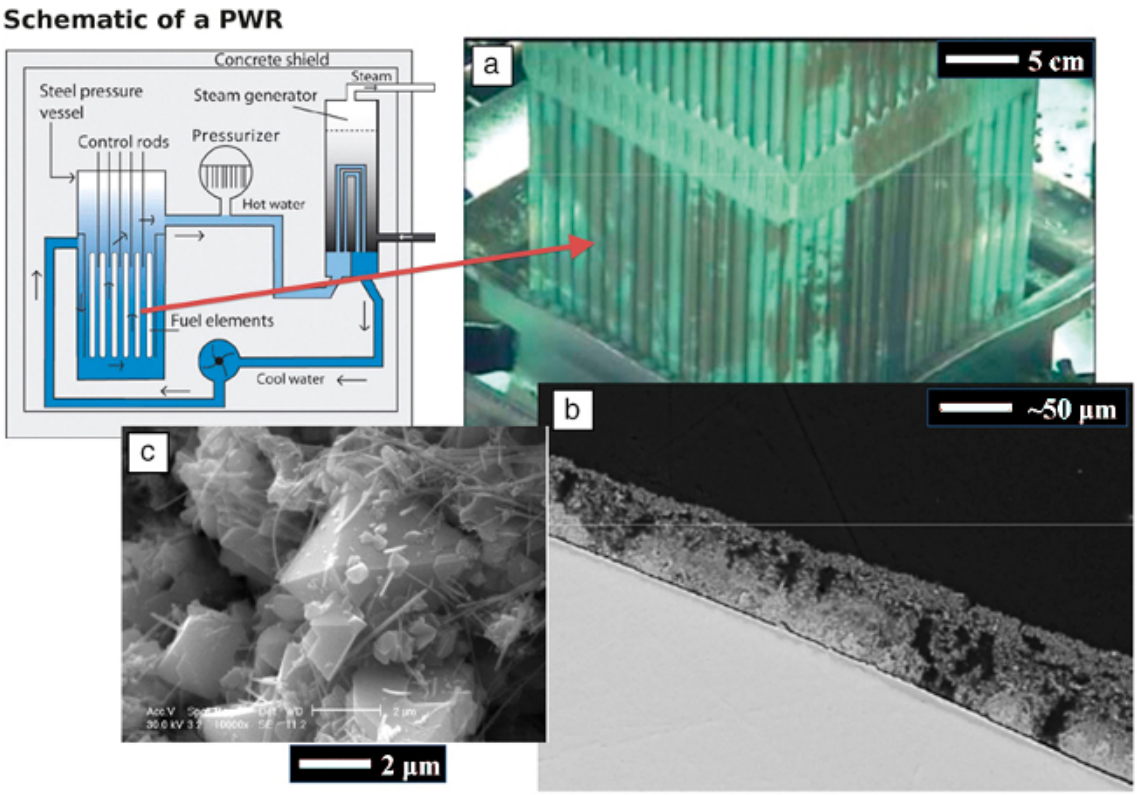

Figure 1: Multiscale Images of CRUD in PWRs [2], showing (a) Appearance of CRUD on fuel cladding rods as a brownish deposit layer (b) Microporous CRUD structure showing boiling chimneys (dark) and porous structure, and (c) Examples of CRUD crystalline particulate constituents. Please click here to view a larger version of this figure.

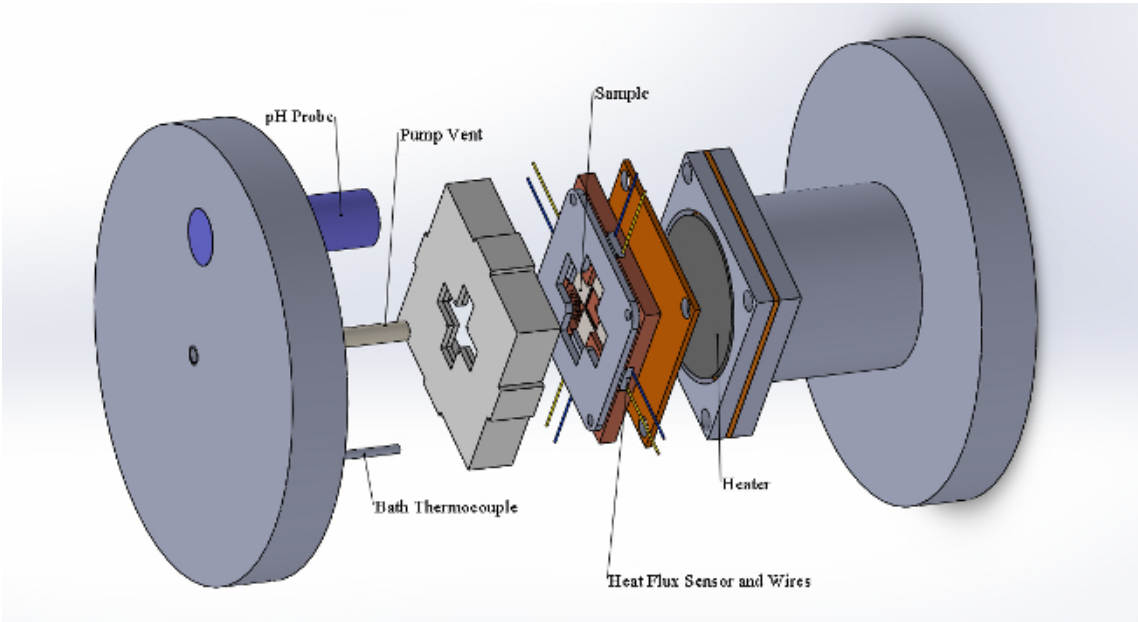

Figure 2: Pool Boiling Experimental Facility Diagram. Please click here to view a larger version of this figure.

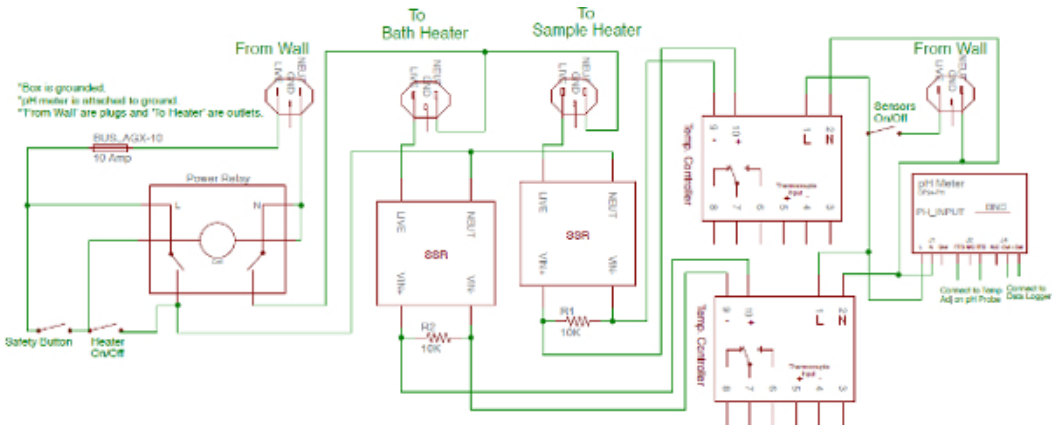

Figure 3: Pool Boiling Facility Control Box Diagram. Please click here to view a larger version of this figure.

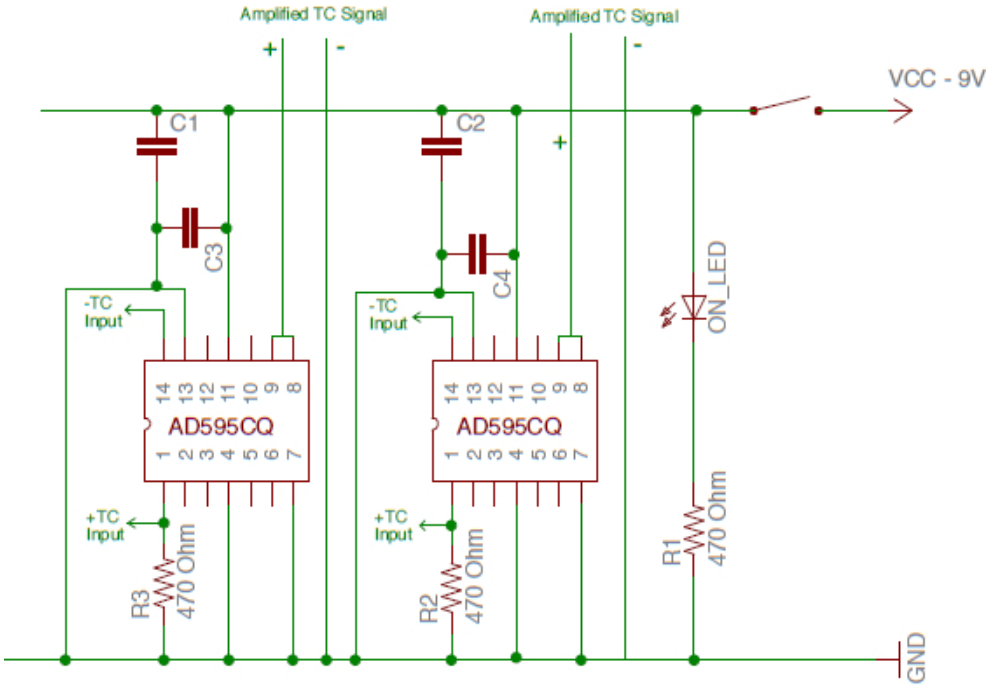

Figure 4: Thermocouple Amplification Circuit Diagram. Please click here to view a larger version of this figure.

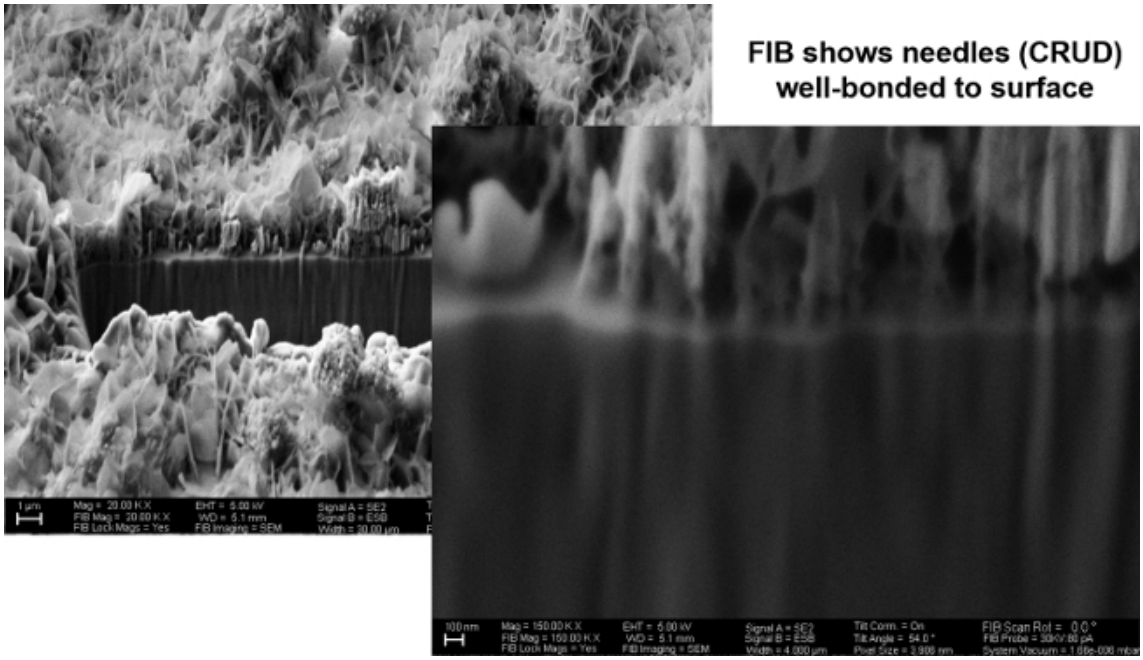

Figure 5: SEM/FIB Image of CRUD Growth on TiO_2, 20,000x & 150,000x. Please click here to view a larger version of this figure.

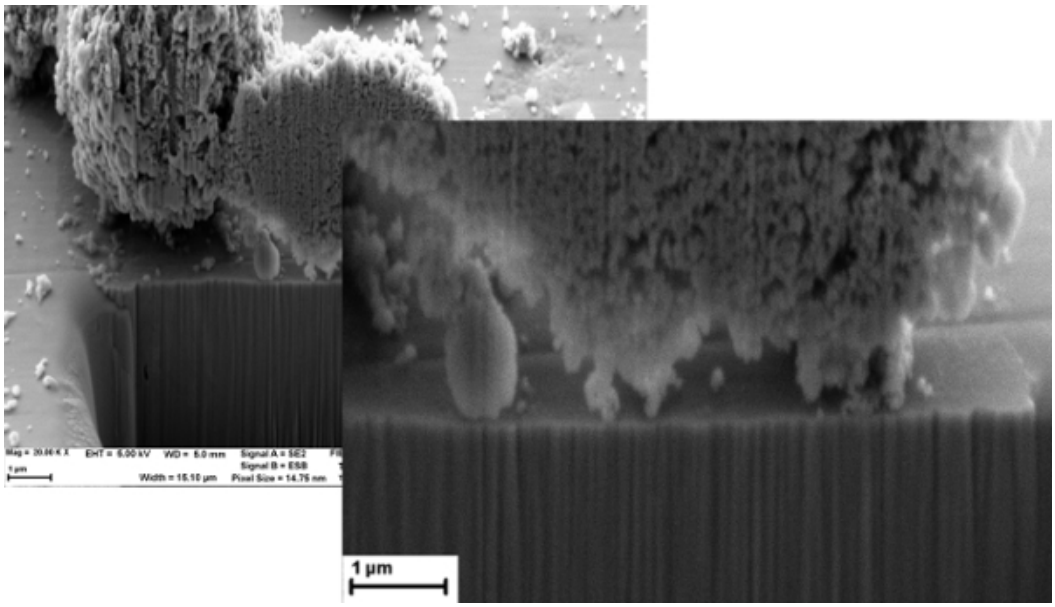

Figure 6: SEM/FIB Image of CRUD Growth on ZrC, 5,000x. Please click here to view a larger version of this figure.

Figure 7: SEM/FIB Image of CRUD. These images show an Omni Probe in the FIB rolling a large piece of CRUD that had deposited, but not adhered to the surface. Please click here to view a larger version of this figure.

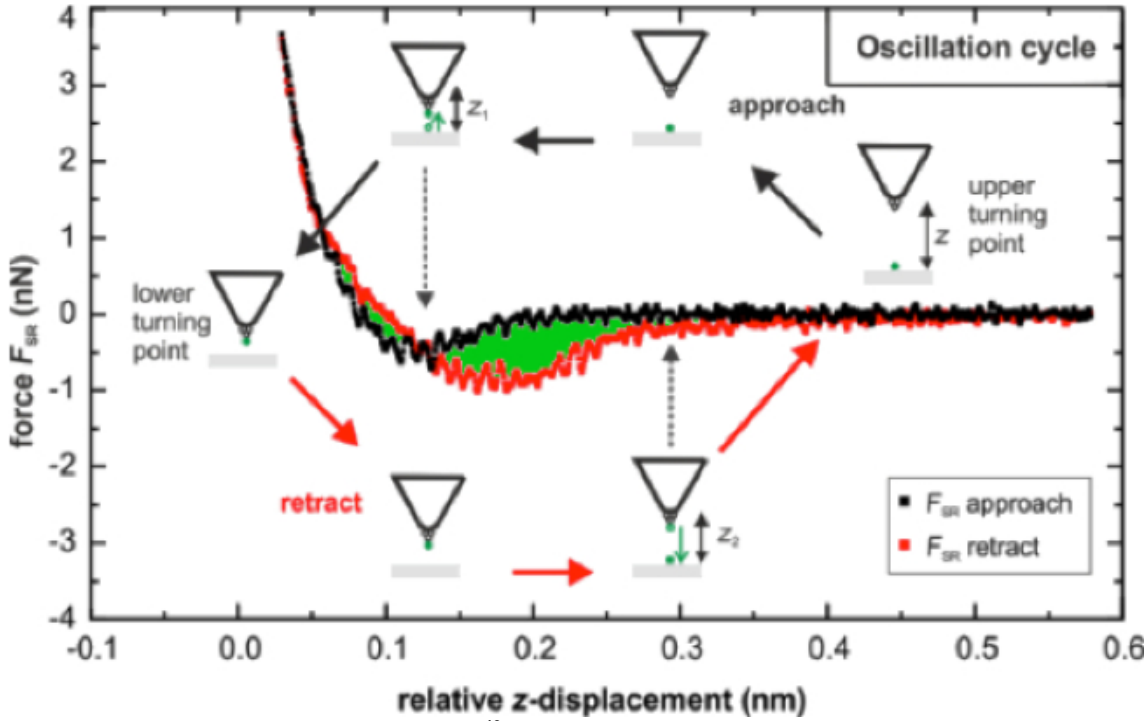

Figure 8: Example AFM-FS Single Force Curve [13]. The black curve represents loading, while the red curve represents unloading. The green area gives a quantitative estimate of adhesion energy. Please click here to view a larger version of this figure.

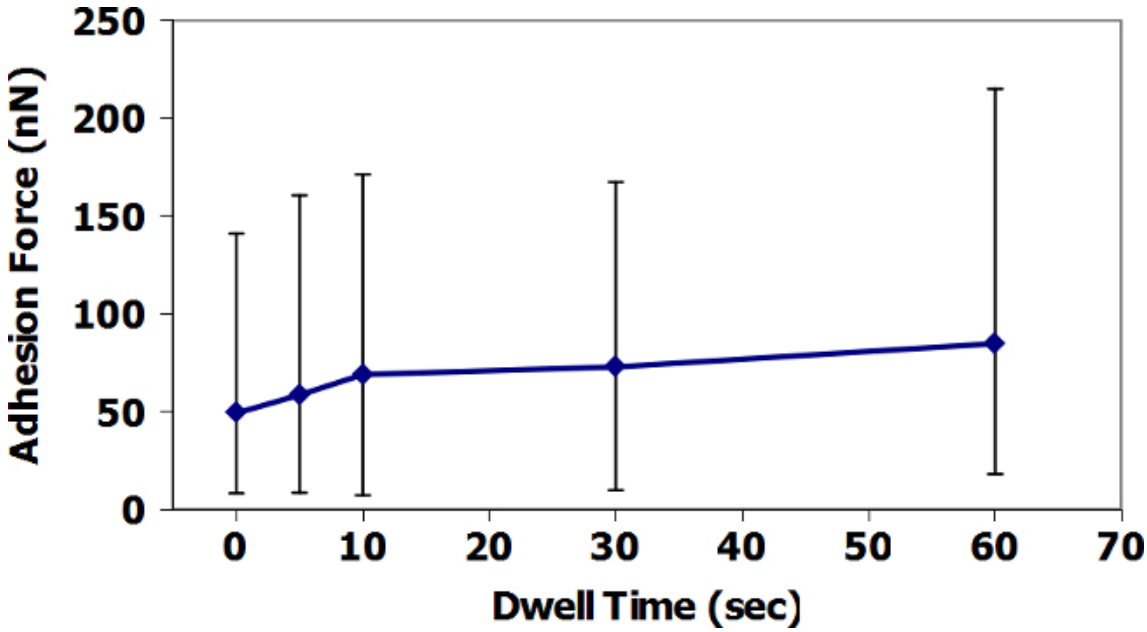

Figure 9: AFM-FS measurement of the adhesion of Fe_3O_4 tip to TiO_2 in Air. Data are averages of 36 measurements at times of 0-30 s dwell time, and 16 measurements at times of 60 s. Error bars show the minimum and maximum of all measurements taken at each dwell time. Please click here to view a larger version of this figure.

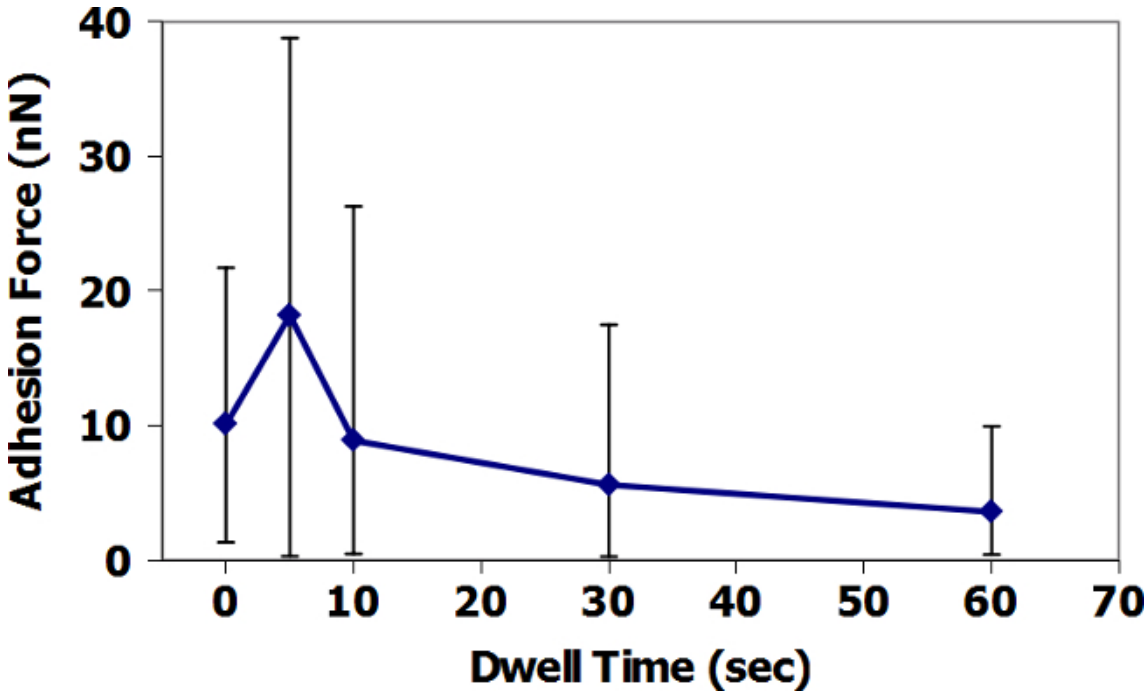

Figure 10: AFM-FS measurement of the adhesion of Fe_3O_4 tip to TiO_2 in Water. Data are averages of 36 measurements at times of 0-30 s dwell time, and 16 measurements at times of 60 s. Error bars show the minimum and maximum of all measurements taken at each dwell time. Please click here to view a larger version of this figure.

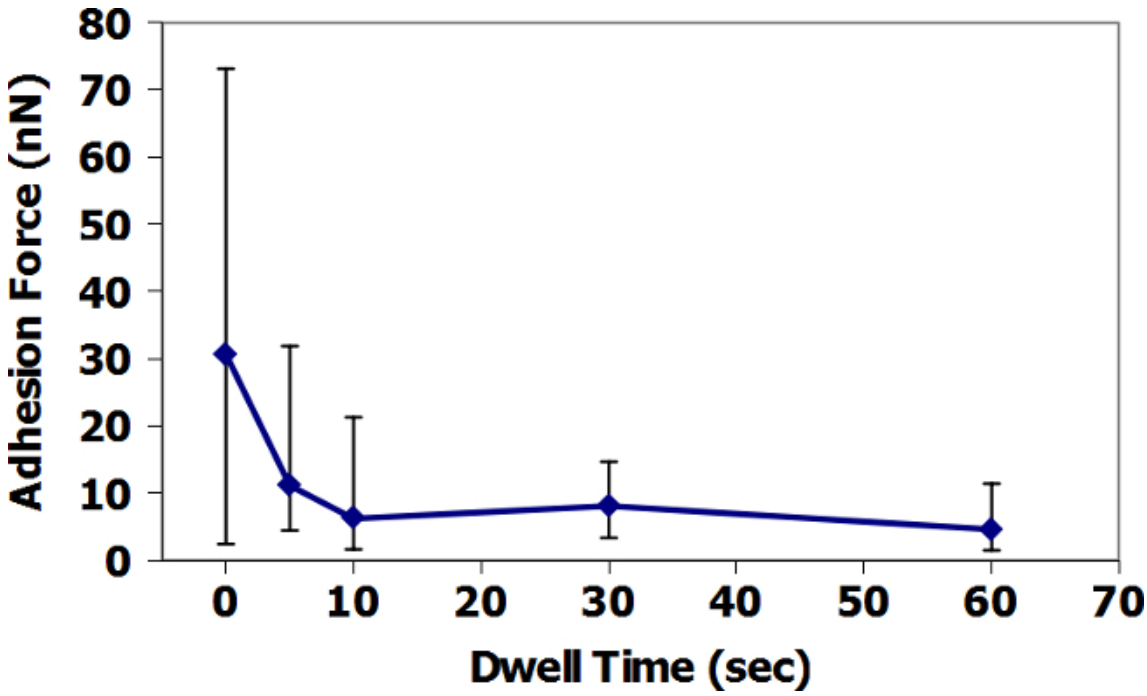

Figure 11: AFM-FS measurement of the adhesion of Fe_3O_4 tip to ZrC in Air. Data are averages of 36 measurements at times of 0-30 s dwell time, and 16 measurements at times of 60 s. Error bars show the minimum and maximum of all measurements taken at each dwell time. Please click here to view a larger version of this figure.

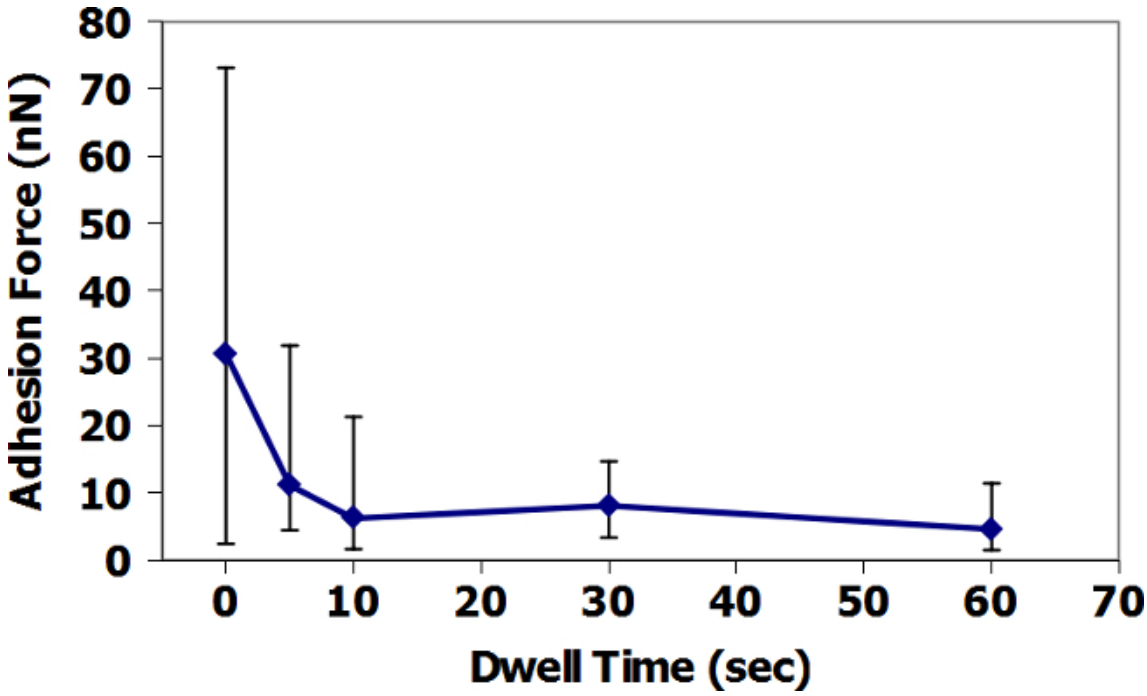

Figure 12: AFM-FS measurement of the adhesion of Fe_3O_4 tip to ZrC in Water. Data are averages of 36 measurements at times of 0-30 s dwell time, and 16 measurements at times of 60 s. Error bars show the minimum and maximum of all measurements taken at each dwell time. Please click here to view a larger version of this figure.

Discussion

This facility has several features that will produce reliable and useful results. First, the vertical orientation of the sample surface prevents solution precipitates from depositing on the surface, as was observed in **Figures 5-6**. Particularly important are the heat flux sensors, used to directly measure heat flux by differences in thermocouple height vs. temperature, rather than back-calculating a heat flux just from temperature measurements. This helps to further ensure experimental repeatability. Finally, the small water circulation pump prevents film boiling from occurring and promotes sub-cooled nucleate boiling, which is the true condition under which CRUD develops in reactors. Sonicating the simulated PWR water also prevents particles from falling out of solution during boiling. Once again, while this facility is specialized to work with CRUD, many of its traits could be used in other fouling growth experiments. The use of the small amplifying circuit in **Figure 4** and a credit-card sized datalogger is a small, simple feature that is applicable for any experiment that collects data electronically, replacing an entire computer and monitor with a circuit board the size of a credit card.

The use of AFM for force spectroscopy can provide repeatable experimental data of adhesion between varieties of dissimilar materials quickly and efficiently. In the procedure shown here, the AFM is outfitted with a tip specifically suited for our research needs. While this procedure is applied to the adhesion of CRUD on a sample, with a variability of tip sizes, shapes, and materials, the procedure shown here is applicable to any problem where the adhesion between two materials at the atomic level in air or in any optically transparent fluid may be useful. AFM-FS has already been used to quantify adhesion and debonding forces between cells [14], organic molecules on glass [15], and between dissimilar solids [16].

For each installation of the chip with the cantilever and tip, the deflection InvOLS and the spring constant will be slightly different, in part because of slight differences in how it is mounted, and in part because the ambient humidity and temperature may also have changed. Recent experimentally validated models have quantified the change in adhesion of AFM-FS measurements as a function of humidity and surface/tip compositions [17]. However, with the ability of the AFM to complete large numbers of measurements quickly, statistically significant results can easily be ascertained.

Figures 9-12 all show a significant decrease in adhesion measurements from air to water. This is to be expected as the decrease of AFM measurements in water with respect to air is a well-documented phenomenon [22]. The presence of conductive water, which contains H_3BO_3 and LiOH, likely eliminates any electrostatic forces present in the AFM-FS in-air measurements. The in-water data also represent conditions more realistic to those found in a PWR. Even so, the data in air and in water show relative correspondence, even though the absolute magnitudes of the in-water data are lower. Because these measurements represent the critical, quantitative data in this procedure, proper measurement techniques in Step 6 are critical to acquiring the data in this procedure. In particular, calibrating the individual spring constants of each tip, in air and in water, represent the largest potential sources of experimental error, and should not be omitted.

Looking at the results from the AFM and the FIB together, it is clear that the adhesion force is likely a significant factor in the growth of CRUD on each substrate. In both air and simulated PWR water, the TiO_2 AFM-FS measurements are consistently higher than those on ZrC. In **Figure 5,** the CRUD is tightly bound to the TiO_2 substrate, while in **Figure 6**, the CRUD sits on a few nanoparticles that appear to rest on the surface of the ZrC substrate, creating a far weaker bond if any at all. These preliminary data suggest that the AFM-FS measurements can predict relative bond strength of CRUD, or any fouling deposit, to candidate anti-fouling substrates. Here, the AFM-FS results have been corroborated by simulated growth of CRUD. The AFM-FS measurements can be extremely useful in providing an initial screening test for coatings or surface modifications

that can limit CRUD growth in nuclear reactors. While this method of AFM measurement and accelerated fouling growth is used here for fouling in nuclear reactors, it can be easily applied to find protective coatings for fouling in many other applications, or to find a substrate the will promote growth of a mineral or crystal.

Disclosures

The authors have nothing to disclose.

Acknowledgements

The authors gratefully acknowledge funding by the Electric Power Research Institute (EPRI)'s PWR Technical Advisory Committee (P-TAC), under grant number 00-10001674. The authors also gratefully acknowledge a donation of Zircaloy-4 material by ATI Wah-Chang, Inc.

References

1. Müller-Steinhagen, H., Malayeri, M.R., Watkinson, A.P. Fouling of Heat Exchangers - New Approaches to Solve an Old Problem. *Heat Transf. Eng.* **26** (1), 1-4 (2005).
2. Short, M. P., Gaston, D., Stanek, C., Yip, S. A Perspective on Nuclear Materials: The Quest for Scientific Advances with Technological Impact. *MRS-B.* **39** (1), 71-77, (2014).
3. Hillner, E., Franklin, D.G., Smee, J.D. Long-term corrosion of Zircaloy before and after irradiation. *J. Nucl. Mater.* **278** (2-3), 334-345 (2000).
4. Short, M.P., et al., Multiphysics Modeling of Porous CRUD Deposits in Nuclear Reactors. *J. Nucl. Mater.* **443** (1-3), 579-587 (2013).
5. Gaston, D., et al. Physics-based multiscale coupling for full core nuclear reactor simulation. *Ann. Nucl. Ener.* (In Press), (2014).
6. PWR Axial Offset Anomaly (AOA) Guidelines, Revision 1, *Technical Report.*1008102, EPRI, Palo Alto, CA (2004).
7. Byers, W.A., Paramonov, D.V., Dzodzo, M.B., Karoutas, Z.E., Young, M.Y. Crud-resistant nuclear fuel cladding. *US Patent. 6813329 B1.* (2004).
8. PWR Primary Water Chemistry Guidelines Committee. PWR Primary Water Chemistry Guidelines. *Technical Report TR-105714.* EPRI, Palo Alto, CA (1999).
9. International Atomic Energy Agency (IAEA). Review of Fuel Failures in Water Cooled Reactors. *IAEA Nuclear Energy Series No. NF-T-2.1.* 54 (2010).
10. Leigh, L. *Controlling CRUD Vapor Chimney Formation in LWRs Through Surface Modifcation. M.S. Thesis.* Massachusetts Institute of Technology (2014).
11. Millett, P. PWR Primary Water Chemistry Guidelines: Revision 4, *Technical Report EPRI TR-105714-V1R4.* EPRI, Palo Alto, CA (1999).
12. Yeon, J., Jung, Y., Pyun, S. Deposition behaviour of corrosion products on the Zircaloy heat transfer surface. *J. Nucl. Mater.* **354** (1-3), 163-170 (2006).
13. Lange, M., van Vorden, D., Moller, R. A measurement of the hysteresis loop in force-spectroscopy curves using a tuning-fork atomic force microscope. *Beilstein J. Nanotech.* **3**, 207-212 (2012).
14. Liu, K.K, Siamantouras, E., Squires, P., Hills, Cl. Investigating viscoelastic effects on cell adhesion using Atomic Force Microscopy. In: *50th Mechanics and Physics of Biological Cells' symposium.* Society of Engineering Science, Rhode Island, USA (2013).
15. Macchietto, S., et al. Fouling in Crude Oil Preheat Trains: A Systematic Solution to an Old Problem. *Heat Trans. Eng.* **32** (3-4), 197-215 (2011).
16. Jaiswal, R.P., Kumar, G., Kilroy, C.M., Beaudoin, S.P. Modeling and Validation of the van der Waals Force During the Adhesion of Nanoscale Objects to Rough Surfaces: A Detailed Description. *Langmuir.* **25** (18), 10612-10623 (2009).
17. Chen, S.C., Lin, J.F. Detailed modeling of the adhesion force between an AFM tip and a smooth flat surface under different humidity levels. *J. Micromech. Microeng.* **18** (11), 115006 (2008).
18. Meyer, E. Atomic Force Microscopy. *Progress Surf. Sci.* **41** (1), 3-49 (1992).
19. Xie, X., Chung, H., Sow, C., Wee, A. Nanoscale materials patterning and engineering by atomic force microscopy nanolithography. *Mater. Sci. Eng. R.*, **54** (1-2), 1-48 (2006).
20. Chen, J. On the Interaction between Fuel Crud and Water Chemistry in Nuclear Power Plants. *Technical Report SKI Report 00:5.* Statens Kärnkraftinspektion (Swedish Nuclear Power Inspectorate, SKI) (2000).
21. Song, M.C., Lee, K.J. A study on a magnetic separation of radioactive corrosion products from NPP using permanent magnets. *Nucl. Eng. Des.* **229** (1), 101-111 (2004).
22. Weisenhorn, A.L., Hansma, P.K, Albrecht, T.R., Quate, C.F. Forces in atomic force microscopy in air and water. *Appl. Phys. Lett.* **54**, 2651-2653 (1989).
23. Lévy, R., Maaloum, M. Measuring the spring constant of atomic force microscope cantilevers: thermal fluctuations and other methods. *Nanotechnology.* **13** (1), 33-37 (2002).

